International Journal of
Molecular Sciences

MDPI

Article

Anti-Virulence Strategy of Novel Dehydroabietic Acid Derivatives: Design, Synthesis, and Antibacterial Evaluation

Puying Qi, Na Wang, Taihong Zhang, Yumei Feng, Xiang Zhou *, Dan Zeng, Jiao Meng, Liwei Liu, Linhong Jin and Song Yang

National Key Laboratory of Green Pesticide, Key Laboratory of Green Pesticide and Agricultural Bioengineering, Ministry of Education, Center for R&D of Fine Chemicals of Guizhou University, Guiyang 550025, China
* Correspondence: zhoux1534@163.com or xiangzhou@gzu.edu.cn

Abstract: Anti-virulence strategies are attractive and interesting strategies for controlling bacterial diseases because virulence factors are fundamental to the infection process of numerous serious phytopathogenics. To extend the novel anti-virulence agents, a series of dehydroabietic acid (DAA) derivatives decorated with amino alcohol unit were semi-synthesized based on structural modification of the renewable natural DAA and evaluated for their antibacterial activity against *Xanthomonas oryzae* pv. *oryzae* (*Xoo*), *Xanthomonas axonopodis* pv. *citri* (*Xac*), and *Pseudomonas syringae* pv. *actinidiae* (*Psa*). Compound **2b** showed the most promising antibacterial activity against *Xoo* with an EC_{50} of 2.7 μg mL^{-1}. Furthermore, compound **2b** demonstrated remarkable control effectiveness against bacterial leaf blight (BLB) in rice, with values of 48.6% and 61.4% for curative and protective activities. In addition, antibacterial behavior suggested that compound **2b** could suppress various virulence factors, including EPS, biofilm, swimming motility, and flagella. Therefore, the current study provided promising lead compounds for novel bactericides discovery by inhibiting bacterial virulence factors.

Keywords: natural products; pesticide discovery; dehydroabietic acid; antibacterial activity; virulence factors

Citation: Qi, P.; Wang, N.; Zhang, T.; Feng, Y.; Zhou, X.; Zeng, D.; Meng, J.; Liu, L.; Jin, L.; Yang, S. Anti-Virulence Strategy of Novel Dehydroabietic Acid Derivatives: Design, Synthesis, and Antibacterial Evaluation. *Int. J. Mol. Sci.* **2023**, *24*, 2897. https://doi.org/10.3390/ijms24032897

Academic Editor: Chiarelli Laurent

Received: 27 December 2022
Revised: 27 January 2023
Accepted: 28 January 2023
Published: 2 February 2023

1. Introduction

Plant diseases are significant threats to crop products worldwide due to the diverse bacterial virulence factors (VFs) promoting pesticide resistance. Rice is the main cash crop worldwide. However, *Xanthomonas oryzae* pv. *oryzae* (*Xoo*), which causes rice bacterial leaf blight (BLB), resulted in 20–60% yield losses during the post-pandemic period [1–3]. VFs significantly contribute to the BLB outbreak and are the main cause of pesticide resistance to traditional bactericides.

Instead of existing as planktonic cells, pathogens predominantly survived in the environment containing affluent biofilms, contributing significantly to their pathogenicity in natural environments. Bacterial infections are caused by numerous virulence factors, such as biofilm, extracellular polysaccharide (EPS), swimming motility, flagella, etc. The literature revealed that approximately 80% of bacterial infections involve biofilm that promotes resistance [4–7]. Meanwhile, EPS is a key element of bacterial biofilm and enhances cell adhesion on the surface of plants [8–10]. Additionally, swimming motility during the infection cycle allows bacteria to travel away from the harmful environment and into the plant tissue, which they can quickly colonize [6]. Swimming motion and bacterial flagella are closely related [11,12], as many bacteria use flagellum for swimming motility [10]. It is clear that VFs are important for bacterial pathogens and are sometimes required for infections [13]. Thus, discovering bacterial virulence inhibitors based on natural products is an appealing method for managing persistent bacterial diseases effectively.

The inhibiting bacterial mechanisms of bioactive natural products and their derivatives are well-established [14–17]. Notably, natural dehydroabietic acid (DAA) and its derivatives

exhibit a broad range of biological activities, and it is a significant renewable forestry resource [17]. As shown in Figure 1, some dehydroabietic acid derivatives had outstanding antibacterial and antibiofilm activity [18–21]. Meanwhile, the amino alcohol unit exists widely in some drugs and antibacterials. Therefore, the above-mentioned compounds with amino alcohol and DAA moieties demonstrated strong antibacterial activities [14,22,23] and were used to develop pesticides to control several plant diseases. In this work, to excavate new anti-virulence agents, a series of amino alcohol-DAA compounds were prepared by adding an amino alcohol moiety to a DAA natural skeleton. The evaluation of the antibacterial mechanism also suggested that the DAA derivative **2b** functioned as a potential virulence factor inhibitor for regulating rice BLB.

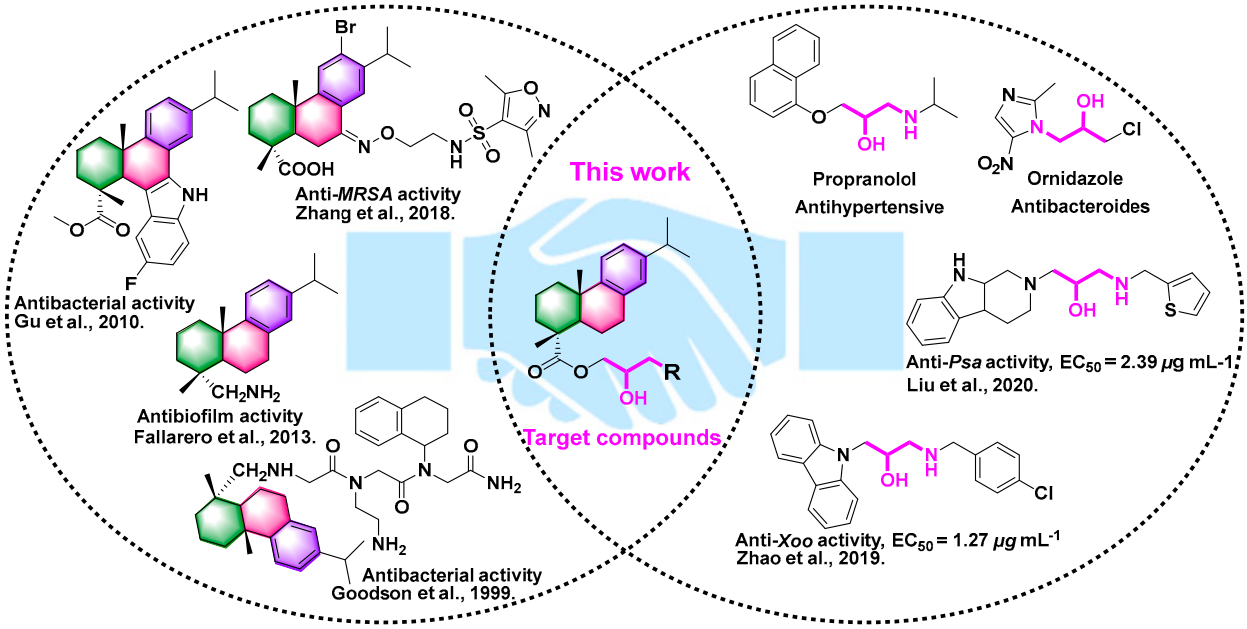

Figure 1. Some commercial and reported bioactive structures with an amino alcohol moiety and dehydroabietic acid and the method for producing target molecules [15,18–21,24].

2. Results and Discussion

2.1. Synthesis of DAA Derivatives

According to previous methods [14,22–24], a series of DAA derivatives with amino alcohol moiety were exquisitely synthesized using combinatorial chemistry. The design concept of the target compounds is shown in Figure 1. Intermediate 1 was obtained by introducing epoxybromopropane, and target compounds were synthesized through an epoxy ring opening reaction. The detailed experimental protocol for synthesizing compounds was found in the supporting information (The spectra data of title compound was displayed in Figures S1–S56).

2.2. Antibacterial Activities Evaluation of Target Compounds

Some target compounds in Figure 2 and Table 1 exhibited strong antibacterial activity against *Xoo*. The inhibition ratios of compounds **2a**–**2c**, **2i**–**2m**, and **2o** against *Xoo* were 91.7%, 92.3%, 90.7%, 88.2%, 85.6%, 91.4%, 89.6%, 89.7%, and 91.9% at a concentration of 100 μg mL^{-1}. Meanwhile, these compounds displayed excellent biological activities against *Xoo* at a dose of 50 μg mL^{-1}. However, compounds **2d**, **2e**, **2f**, **2g**, and **2n** almost displayed negligible or no bioactivities at 50 and 100 μg mL^{-1}. Interestingly, compared with compound **2h**, when a substituent group in the *N*-heterocyclic portion was lacking, compounds showed medium bioactivities, exampled by **2p**.

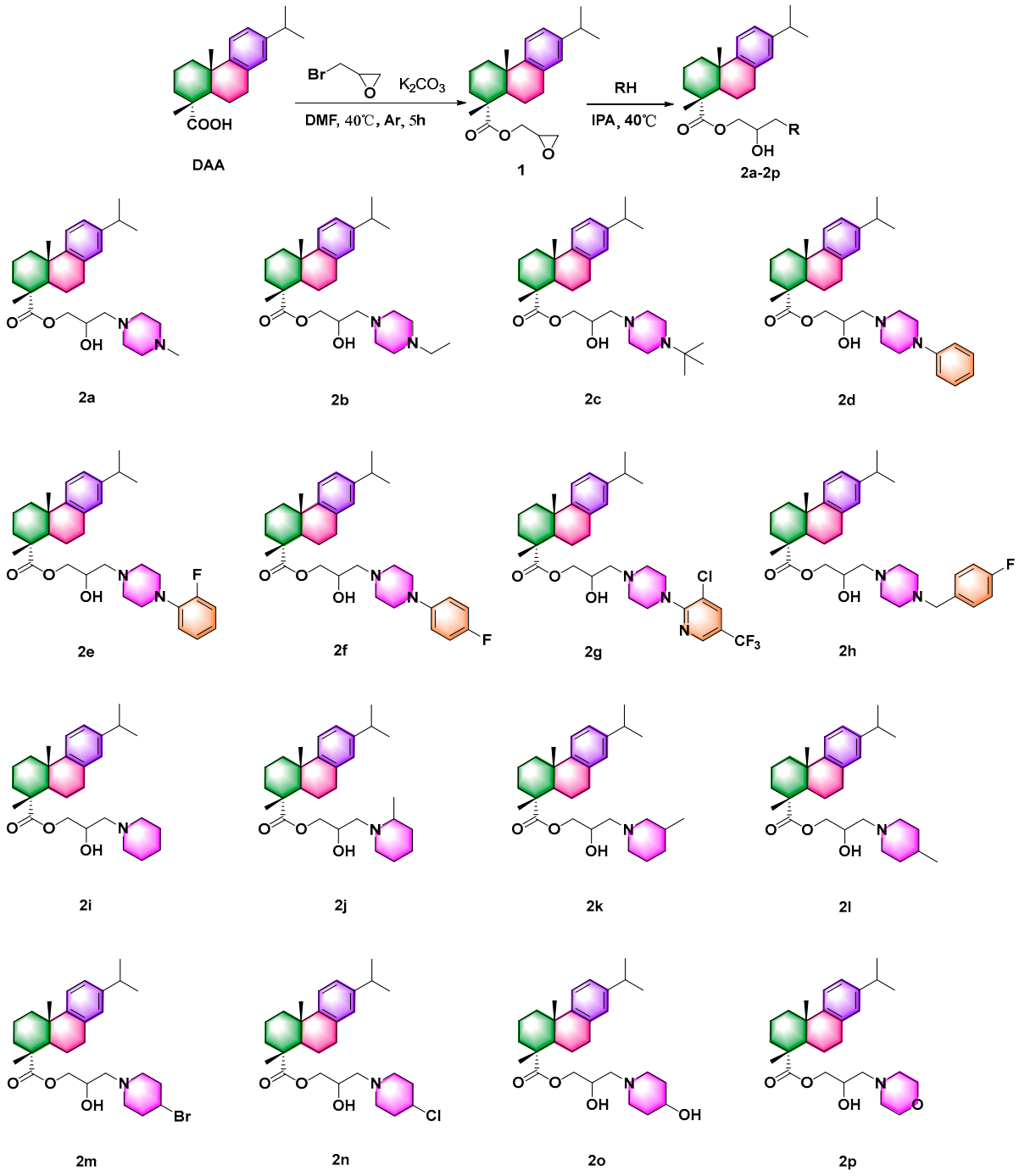

Figure 2. Synthesis route of target molecules **2a**–**2p**.

Based on the results mentioned above, additional antibacterial activity assays were carried out on *Xanthomonas axonopodis* pv. *citri* (*Xac*) and *Pseudomonas syringae* pv. *actinidiae* (*Psa*). Compounds **2a**, **2b**, **2c**, **2f**, **2i**, **2j**, **2k**, **2l**, and **2o** had strong bioactivities against *Xac* with inhibition ratios of 88.6%, 89.7%, 89.0%, 86.7%, 83.5%, 87.4%, 83.3%, 85.1%, and 89.1% at a concentration of 100 μg mL^{-1} (Table 1). However, as the control molecule, cyclohexanecarboxylic acid aminoalcohol derivatives did not exhibited antibacterial activity (Table S1), suggesting that retional design of title compounds can achieve the outstanding antibacterial activity. Additionally, these compounds demonstrated significant in vitro inhibitory activity against *Xac* at 50 μg mL^{-1}. Furthermore, **2h**, **2m**, **2n**, and **2p** exhibited moderate biological activity, while the other target compounds exhibited low inhibitory

activity. Nevertheless, all compounds displayed moderate or no antibacterial activity against *Psa* at 100 and 50 μg mL^{-1}.

Table 1. Antibacterial bioactivity of compounds against the phytopathogenic bacteria *Xoo*, *Xac*, and *Psa* in vitro.

Compds	Inhibition Ratio (%)					
	Xoo		*Xac*		*Psa*	
	100 μg mL^{-1}	50 μg mL^{-1}	100 μg mL^{-1}	50 μg mL^{-1}	100 μg mL^{-1}	50 μg mL^{-1}
DAA	43.9 ± 2.7	38.4 ± 3.4	56.9 ± 3.4	44.1 ± 12.6	39.8 ± 9.5	34.5 ± 10.2
2a	91.7 ± 0.8	91.6 ± 0.3	88.6 ± 1.5	87.5 ± 0.4	48.3 ± 6.8	41.2 ± 1.6
2b	92.3 ± 0.3	91.0 ± 0.3	89.7 ± 0.2	89.4 ± 0.3	40.6 ± 5.1	38.1 ± 7.5
2c	90.7 ± 0.3	89.2 ± 1.4	89.0 ± 1.3	85.9 ± 1.5	54.3 ± 7.5	49.6 ± 6.8
2d	0	0	0	0	0	0
2e	0	0	0	0	0	0
2f	0	0	86.7 ± 0.1	85.9 ± 0.1	17.7 ± 3.1	16.8 ± 7.7
2g	10.7 ± 3.8	0	0	0	0	0
2h	65.9 ± 0.5	64.2 ± 0.2	41.8 ± 7.0	37.2 ± 5.2	0	0
2i	88.2 ± 0.7	79.0 ± 0.8	83.5 ± 1.1	79.0 ± 2.9	53.2 ± 7.1	50.1 ± 5.5
2j	85.6 ± 0.4	84.3 ± 0.3	87.4 ± 1.8	84.0 ± 0.5	58.1 ± 0.3	52.6 ± 4.2
2k	91.4 ± 0.1	88.9 ± 0.4	83.3 ± 0.8	82.6 ± 0.9	36.0 ± 1.6	7.3 ± 5.0
2l	89.6 ± 3.1	87.5 ± 1.2	85.1 ± 2.4	82.1 ± 1.4	55.2 ± 1.5	50.1 ± 0.7
2m	89.7 ± 0.6	89.4 ± 1.2	47.2 ± 5.4	44.3 ± 0.7	47.5 ± 9.9	46.6 ± 1.6
2n	11.3 ± 2.5	0	48.4 ± 2.7	45.0 ± 1.2	45.9 ± 2.8	40.8 ± 8.5
2o	91.9 ± 0.9	91.8 ± 0.3	89.1 ± 1.5	88.5 ± 0.5	51.0 ± 5.8	48.2 ± 5.5
2p	62.2 ± 3.5	54.5 ± 1.2	48.7 ± 9.2	40.0 ± 3.9	30.4 ± 1.2	21.8 ± 1.3
TC	85.1 ± 5.3	46.8 ± 2.2	56.3 ± 3.2	32.3 ± 2.1	63.1 ± 6.2	33.6 ± 2.2

Thiodiazole copper (TC), Xanthomonas oryzae pv. oryzae (Xoo), Xanthomonas axonopodis pv. citri (Xac), and Pseudomonas syringae pv. actinidiae (Psa).

The effective concentration for 50% of maximal effect (EC_{50}) of these compounds against *Xoo* was determined based on the excellent antibacterial activity of several compounds against *Xoo*. Compound **2b** exhibited the greatest inhibitory activity, with a value of 2.70 μg mL^{-1} (Table 2), and its MIC value was 10.8 μg mL^{-1} (Table S4). Furthermore, compounds **2a**, **2c**, **2h**, **2i**, **2j**, **2k**, **2l**, **2m**, and **2n** showed good inhibitory activities ranging from 3.2–7.0 μg mL^{-1}. The EC_{50} values for each compound were 7.0, 3.2, 5.8, 3.2, 3.6, 4.1, 3.0, and 5.3 μg mL^{-1}. However, compounds **2d** and **2p**, with values of 13.0 and 24.4 μg mL^{-1}, had medium biological activity. None of the other compounds displayed antibacterial activity with EC_{50} values >100 μg mL^{-1}, except compound **2o**; the EC_{50} of compound **2o** was 5.7 μg mL^{-1}. Figure 3 summarizes the structure-activity relationship. The results showed that when three heterocyclic amines substituents were added, the EC_{50} of the target compounds decreased in the following order: piperazine derivatives (*N*-ethylpiperazine title compound with the highest EC_{50}, 2.7 μg mL^{-1}) > piperidine derivatives (EC_{50}, 3.0–5.3 μg mL^{-1}) > morpholine derivatives (EC_{50}, 24.4 μg mL^{-1}). In addition, antibacterial activity tests revealed that adding alkyl substituents to the piperazine ring was beneficial. However, the aromatic groups on the piperazine ring would have poor bioactivity. Furthermore, molecules with the same substituent at different positions of the piperidine ring exhibited different anti-*Xoo* activity, as evidenced by the fact that the EC_{50} of compounds decreased in the order, 4-methyl piperidine derivative (EC_{50} value, 3.0 μg mL^{-1}) > 2-methyl piperidine derivative (EC_{50} value, 3.6 μg mL^{-1}) > 3-methyl piperidine derivative (EC_{50} value, 4.1 μg mL^{-1}). Finally, introducing electron-donating groups were useful, while reduced bioactivity was observed by conducting with electron-withdrawing groups.

Table 2. EC_{50} of highly bioactive compounds against *Xoo*.

Compds	Regression Equation	R^2	EC_{50} (μg mL^{-1})	$EC_{50'}$ (μM)
2a	y = 2.6697x + 2.7486	0.9182	7.0 ± 0.5	15.3
2b	y = 2.0052x + 4.1343	0.9558	2.7 ± 0.3	5.7
2c	y = 1.4267x + 4.5965	0.9369	3.2 ± 0.9	6.4
2d	y = 2.3605x + 2.3735	0.8867	13.0 ± 1.7	25.1
2e			>100	
2f			>100	
2g			>100	
2h	y = 1.0065x + 4.2365	0.9829	5.8 ± 0.7	10.5
2i	y = 2.0242x + 3.9693	0.9066	3.2 ± 0.7	7.2
2j	y = 1.8918x + 3.9619	0.8840	3.6 ± 0.5	8.1
2k	y = 1.9734x + 3.7912	0.9149	4.1 ± 0.8	9.2
2l	y = 1.4200x + 4.5751	0.9630	3.0 ± 0.4	6.7
2m	y = 1.5424x + 3.8815	0.9288	5.3 ± 0.8	10.2
2n			>100	
2o	y = 4.5670x + 1.5782	0.9943	5.7 ± 0.5	12.5
2p	y = 0.6191x + 4.1400	0.9510	24.4 ± 1.2	55.0
TC	y = 5.4033x − 2.3402	0.9621	61.2 ± 5.2	186.6

Thiodiazole copper (TC), *Xanthomonas oryzae* pv. *oryzae* (*Xoo*).

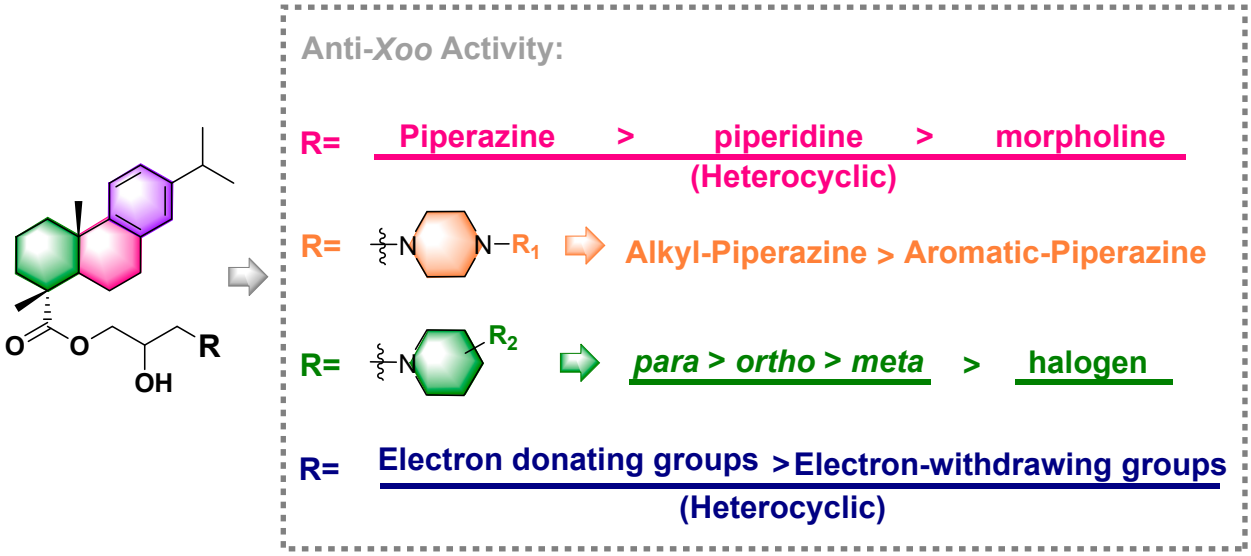

Figure 3. Overall structure-activity relationship analysis of all target compounds.

2.3. Inhibitory Effects of Compound **2b** *on the Xoo-Biofilm Formation and EPS Production*

Biofilm, as one of the important VFs, is a significant and highly conserved structure for the bacterial community that acts as a crucial physical barrier against various complex environmental threats, including pH, temperature changes, host defense, and antibiotics [25–27]. Consequently, biofilm may significantly increase bacterial resistance [28–31] and is responsible for 80% of bacterial infections [4,32]. Additionally, EPS is the main component of the biofilm that promotes adherence to host surfaces [33,34]. However, *Xanthomonas* species such as *Xoo* and *Xanthomonas campestris* pv. *campestris* secreted the EPS known as xanthan gum. Therefore, xanthan gum would be used as a *Xoo* (a kind of *Xanthomonas*) indicator for detecting EPS production. To verify the experimental concentration is suitable, namely, that compound **2b** displayed anti-virulence activity rather than killing activity, the OD_{595} value was assayed (Table S2). Notably, when the dosage was 5.40 μg mL^{-1}, compound **2b** did not show any bactericidal activity. Thus, the biofilm formation assay is carried out.

As shown in Figure 4, compound **2b** demonstrated an outstanding inhibitory effect for *Xoo*-biofilm formation. When concentrations of compound **2b** were 0, 1.35, 2.70, 5.40,

10.8, and 21.6 μg mL^{-1}, respectively, the inhibition rates of bacterial biofilm products were 0, 63%, 69%, 77%, 86%, and 87%, respectively. Furthermore, as displayed in Figure 5, the production of xanthan gum was 225.3, 60.3, 44.3, 24.1, and 1.4 μg mL^{-1} after treatment with compound **2b** at dosages of 0, 1.35, 2.70, 5.40, and 10.8 μg mL^{-1}, respectively. This suggests that compound **2b** might interfere with the biosynthesis process of xanthan gum. In brief, biofilm formation was constantly reduced with increasing concentrations, while the xanthan gum biosynthesis process decreased with increasing concentrations. Therefore, compound **2b** had the potential to inhibit bacterial biofilm formation.

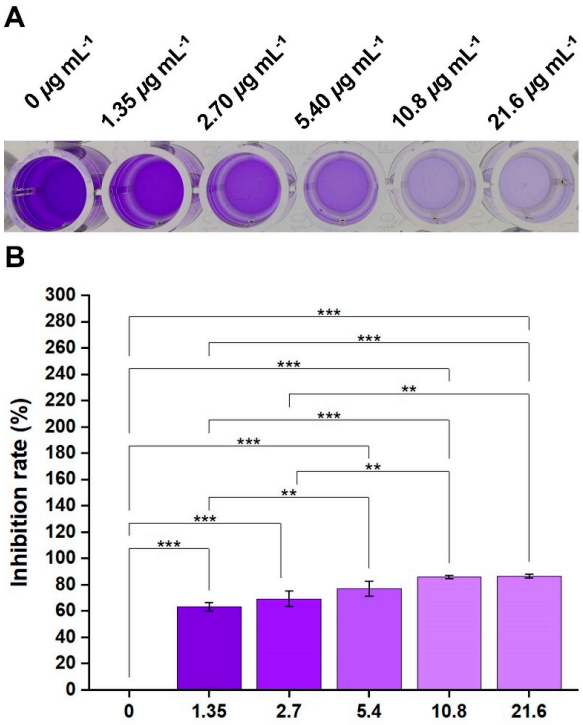

Figure 4. The quantitative assessment of crystal violet revealed the *Xanthomonas oryzae* pv. *oryzae*-biofilm inhibition of compound **2b**. (**A**) Biofilm staining imagins. (**B**) Inhibition rate of biofilm formation. [(**) $p < 0.01$, (***) $p < 0.001$ vs. 0].

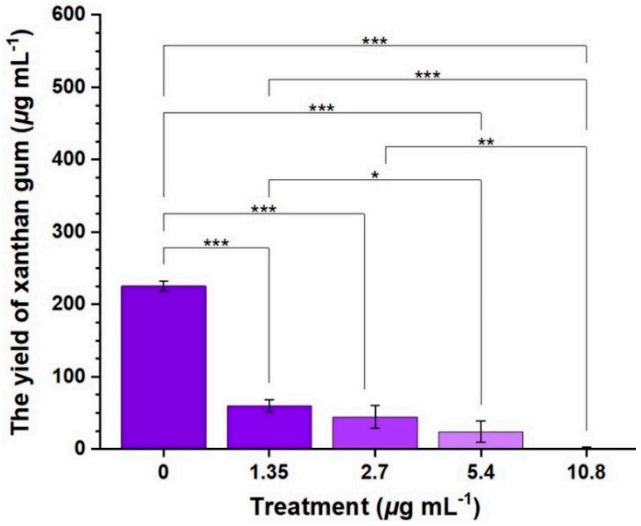

Figure 5. The production of xanthan gum [also known as an extracellular polysaccharide in *Xanthomonas oryzae* pv. *oryzae* (*Xoo*)] in the *Xoo*-biofilm after exposure to compound **2b** [(*) $p < 0.05$, (**) $p < 0.01$, (***) $p < 0.001$ vs. 0].

2.4. The Inhibition Effect of Swimming Motility

Most phytopathogenic bacteria, including *Ralstonia solanacearum* and *Xanthomonas*, display good swimming motility [35], with bacterial swimming being the fastest mode of motility [12]. Swimming motility enables bacteria to sense environmental changes, avoid harmful environmental stressors, and move toward nutrients, consequently markedly enhancing bacterial fitness [36,37]. Figure 6 showed that swimming diameter decreased with increasing doses. The swimming diameters at concentrations of 0, 1.35, 2.70, 5.40, and 10.8 μg mL^{-1} were 13.8, 11.5, 7.7, 3.6, and 0 mm, respectively; bacterial swimming motility was gradually weakened. Compound **2b** inhibited bacterial motility levels, lowered fitness, and decreased infections.

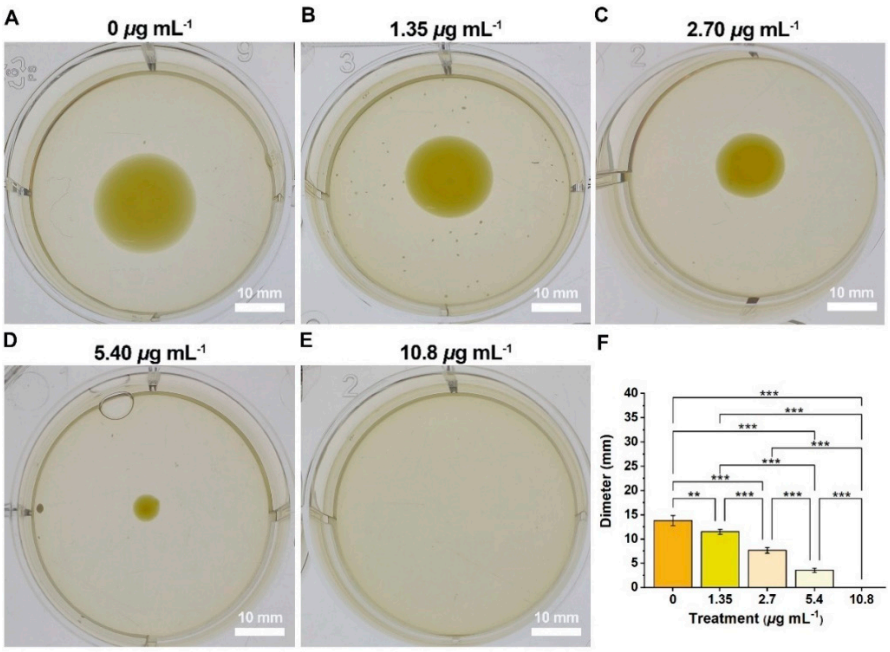

Figure 6. Compound **2b** inhibited the swimming motility of *Xanthomonas oryzae* pv. *oryzae* at concentrations of 0 (**A**), served as blank), 1.35 (**B**), 2.70 (**C**), 5.40 (**D**), and 10.8 (**E**) μg mL^{-1}, and the swimming diameters were presented in (**F**). [(**) $p < 0.01$, (***) $p < 0.001$ vs. 0]. Scale bars are 10 mm.

2.5. The Inhibition Effect of Xoo-Flagellum Assembly

The flagellum is the important bacterial organelle responsible for swimming motility [38], comprising the filament, hook, and basal body [38]. The ability of bacterial cells to move toward beneficial environments and escape harmful environmental stressors, and the swimming motility mediated by the bacterial flagellum, play a significant role in the bacterial infection cycle, increasing the probability of cells interacting with hosts' surfaces [39,40]. The ability was extremely beneficial for enhancing search potency, enabling bacteria to seek advantages and avoid disadvantages. It revealed that a bacterium's virulence toward its host was significantly influenced by flagellum-mediated swimming motility [41,42]. Swimming motility, chemotaxis, and host cell invasion increased the likelihood of bacteria interacting with host organism surfaces during the infection [13]. Furthermore, the mutation of flagella-related genes resulted in a loss of motility, reduction in bacterial colonization, downregulation of host cell immunity, decrease the virulence, and reduction in pathogenicity [13,42]. Thus, the flagellum, which also contains swimming motility, initial attachment, tissue invasion, and biofilm formation, contributes to bacterial virulence and infection [13,42].

As shown in Figure 7, the percentage of flagellum assembly was 0.78, 0.49, and 0.26 at doses of 0, 0.27, and 1.35 μg mL^{-1}. These findings show compound **2b** strongly interfered with the flagellum assembly process at concentrations 0.27 and 1.35 μg mL^{-1}. Moreover,

bacterial flagellum assembly interfered similarly at a dose of 0 μg mL^{-1} (served as a control). The primary cause was that some bacteria had mature flagellum while others were at the initiation or growth stage. The assembly and disassembly of the flagellum, a dynamic nanostructure, was coupled with the cell cycle [43]. Therefore, we can infer that the cells in the initiation and growth stages did not complete the assembly of their flagella. These findings suggested compound **2b** might significantly interfere with bacterial flagellum assembly and cause virulence downregulation.

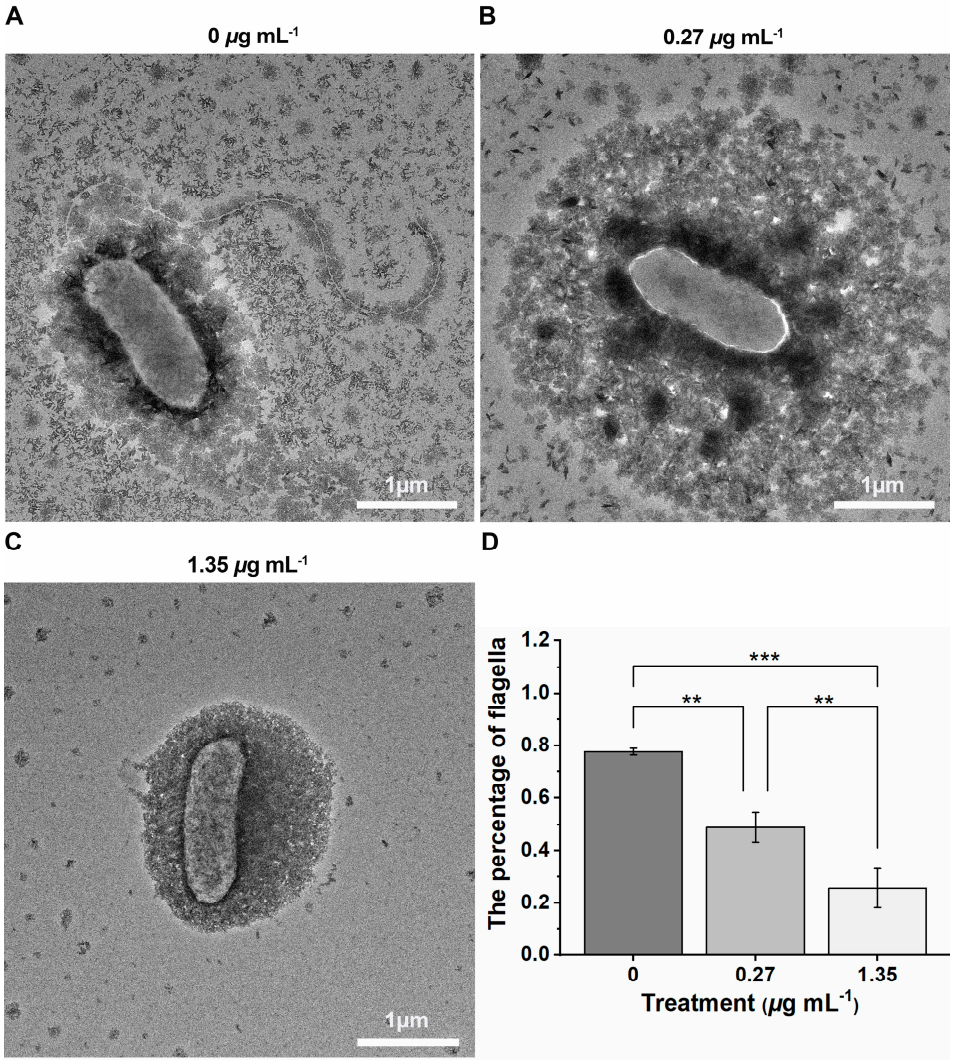

Figure 7. The *Xanthomonas oryzae* pv. *oryzae*-flagella assembly interfered with compound **2b** at doses 0 (**A**), 0.27 (**B**), and 1.35 μg mL^{-1} (**C**), presented in the transmission electron microscope, and the percentage of flagella was showed in (**D**) [(**) $p < 0.01$, (***) $p < 0.001$ vs. 0]. Scale bar = 1 μm.

2.6. Cell Membrane Morphology Analysis

The cell membrane plays a role in nutrient intake, biomacromolecule transportation, and signal transduction, as well as being a considerable barrier to complicate external environmental stresses [31]. Thus, the cell membrane plays a significant role in these physiological and biochemical processes. A loss in bacterial cell membrane integrity results in increased membrane permeability, which impacts cell physiology and metabolism, leading to cytoplasm leakage and cell death [32,44–47]. Additionally, the membrane reportedly plays a crucial role in preserving cell homeostasis, with a loss of membrane integrity leading to the end of the cellular life cycle [30,48]. Figure 7 indicated that compound **2b** affected flagella assembly but not the morphology of cellular membranes. In addition, the properties

of VF inhibitors did not hinder cellular development and proliferation at a low dose of compound **2b**. Therefore, SEM technology was used to analyze the morphology of cell membranes. Figure 8 showed the morphology observation results: bacterial morphology was unchanged after treatment with varying doses of 0, 25, and 50 μg mL^{-1} and showed a smooth surface and rod-shaped structure. As a result, compound **2b** only affected biological processes related to bacterial VFs and did not affect the structure of bacterial cell membranes or interfere with normal cellular growth and proliferation.

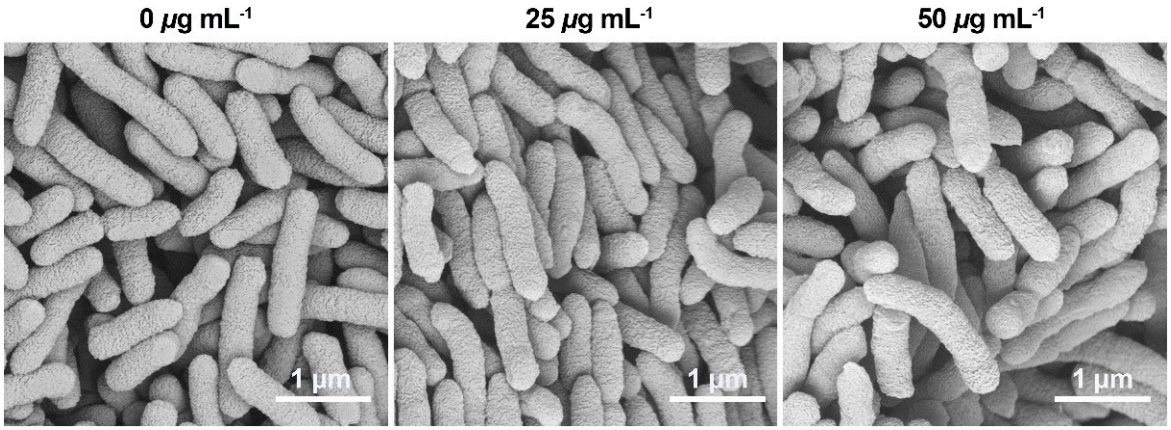

Figure 8. Scanning electron microscope images of the morphology of the *Xanthomonas oryzae* pv. *oryzae* cell membrane induced by compound **2b** at doses 0 (served as blank), 25, and 50 μg mL^{-1} 24 h. Scale bars = 1 μm.

2.7. Pathogenicity of the Xoo Interacted with Compound **2b**

Several VFs strongly correlate with the pathogenicity of infections [49]. VFs secreted by different bacteria are crucial for promoting cell colonization and enhancing pathogenicity during infection [50,51]. Pathogens use several VFs to overcome the host's defense system [52]. Thus, bacterial pathogenicity depends on their ability to secrete numerous VFs [53]. *R. solanacearum* uses various VFs to infect plants and cause a withering phenomenon. EPS, also known as xanthan gum in *Xoo*, lipopolysaccharides, extracellular enzymes (including amylase, endoglucanase, polygalacturonate lyase, and protease), and biofilm are some significant VFs that have been found in many bacteria [54,55]. Additionally, bacterial motility and flagella facilitate cell colonization and adhesion [55]. *Erwinia amylovora* develops many VFs to overcome the plant immune system and facilitate infection [56]. The bacterium *Xanthomonas campestris* pv. *campestris* encodes for type III secretion system-dependent transcription activator-like effectors, among other VFs [54]. Massive VFs may interfere with the host's vascular system and cause wilting symptoms [57]. Cell and tissue damage caused by *Staphylococcus aureus* and *Nocardia adhesion* and invasion are important pathogenetic factors [26]. A thorough analysis revealed that antibacterial peptides reduced bacterial pathogenicity by inhibiting VFs activity [58]. Disrupting the secretion and assembly of VFs has been associated with several anti-virulence compounds, including those that inhibit biofilm formation, lower EPS production, and interfere with initial bacterial adhesion [59]. The mechanism of VFs in host infection has been gradually explored and excavated thanks to advancements in molecular biology techniques and a comprehensive understanding of VFs. Targeting VFs would be a desirable and practical method to eliminate or reduce bacterial pathogenicity and weaken resistance by interfering with virulence biosynthesis processes as opposed to cell death because VFs are crucial for bacterial infections [6,60,61].

Thus, the analysis of *Xoo*-pathogenicity was performed based on the results of the above-mentioned completed experiments, and compound **2b** significantly disrupted *Xoo*-virulence biological processes. As shown in Figure 9, the *Xoo* cells suspension was co-incubated with compound **2b** for one day at the different doses of 0 (referred to as the

control), 0.27, 1.35, and 2.70 μg mL^{-1}. The rice plant was then inoculated with the above-mentioned cell suspension using the leaves clipping method. Subsequently, the *Xoo*-inoculated rice plant was cultured for 14 days. Finally, samples from the control treatment showed more lathy lesions with a length of 11.5 cm. The lesion lengths of other treatments, 0.27, 1.35, and 2.70 μg mL^{-1} were 8.7, 5.9, and 2.9 cm, respectively. As a result of interfering with the manufacture of multiple bacterial VFs, compound **2b** demonstrated the ability to suppress *Xoo*-VFs and strongly reduce bacterial pathogenicity. Compound **2b** would be a potent virulence inhibitor to manage rice BLB successfully.

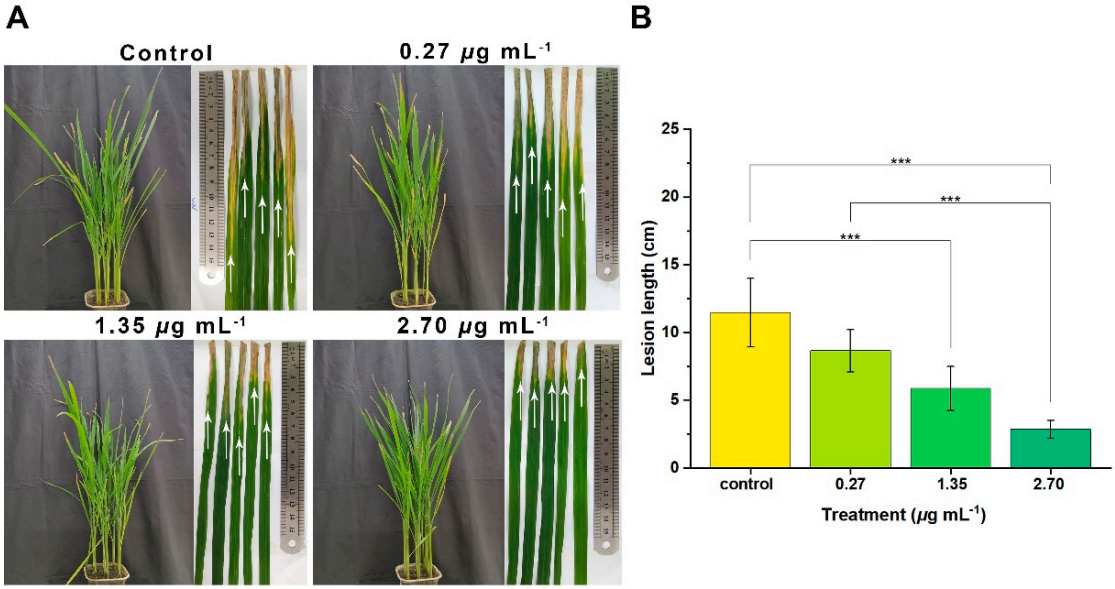

Figure 9. Effects of compound **2b** on the representative *Xanthomonas oryzae* pv. *oryzae*'s (*Xoo*) responses to the rice bacterial leaf blight disease. (**A**) The leaf-clipping method was used to co-incubate rice leaves with the *Xoo* cell suspension after exposure to doses 0 (served as blank), 0.27, 1.35, and 2.70 μg mL^{-1} of compound **2b** for 24 h. (**B**) The length of a lathy lesion of rice leaves was measured in *Xoo* at various doses of compound 2b [(***) $p < 0.001$ vs. 0].

2.8. In Vivo Anti-Xoo Effect of Compound **2b** *Controlling Bacterial Disease at 200 μg mL^{-1}*

Although target compound **2b** demonstrated excellent antibacterial activity and an alluring anti-VFs mechanism, the preservation of the crops was our ultimate goal. Therefore, the antibacterial activity of compound **2b** was investigated in vivo to verify its anti-*Xoo* activity. Compound **2b** demonstrated excellent curative and protective activities, and the control efficiency was 48.6% and 61.4%, respectively (Figure 10 and Table 3). Compound **2b** exhibited significant antibacterial activity in vitro and exceptional control efficiency in vivo.

Table 3. Compound **2b** and TC at 200 μg mL^{-1} in vivo demonstrated both curative and protective activities against rice bacterial leaf blight under greenhouse conditions.

Treatment	Curative Activity (14 Days after Spraying)			Protection Activity (14 Days after Spraying)		
	Morbidity (%)	Disease Index (%)	Control Efficiency (%)	Morbidity (%)	Disease Index (%)	Control Efficiency (%)
2b	100	40.00	48.57	100	30.00	61.43
TC	100	57.78	25.72	100	62.22	20.00
CK	100	77.78	/	100	77.78	/

2b: target compound **2b**; TC: thiodiazole copper; CK: blank control.

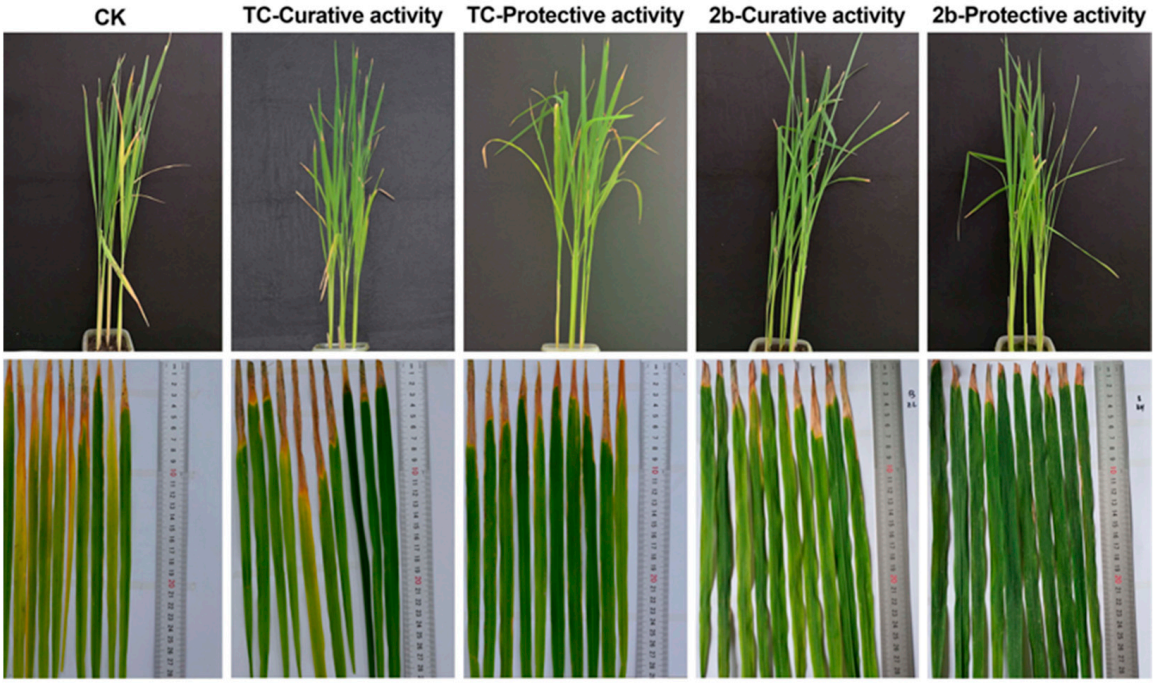

Figure 10. In vivo antibacterial activity of compound **2b** and TC against rice bacterial leaf blight at 0 μg mL^{-1} (served as CK) and 200 μg mL^{-1}; **2b**: target compound **2b**; TC: thiodiazole copper; CK: blank control.

2.9. The Toxicity Evaluation of Compound **2b** *on Rice Leaves at 0, 200, and 500 μg* mL^{-1}

Although compound **2b** showed remarkable antibacterial activity in vitro and in vivo, its phytotoxicity for the target crop remained unknown. Therefore, the phytotoxicity of compound **2b** was assessed at doses of 0, 200, and 500 μg mL^{-1}. As shown in Figure 11 and Table S3, compound **2b** did not affect the normal growth of rice leaves and did not cause any lesions or necrosis. Furthermore, as found in Figure S57, predicting results suggested that the title compounds exhibited acceptable physicochemical properties. Thus, it would be a highly effective and low-risk green pesticide option.

Figure 11. The phytotoxicity assessment of compound **2b** on rice leaves after co-culturing it for seven days at 0, 200, and 500 μg mL^{-1}.

3. Materials and Methods

3.1. Instruments and Chemicals

Thin-layer chromatography plates were used to monitor organic reaction processes (Yantai Jiangyou Silica Development Co., Ltd., Silica HSGF254, Shandong, China) [51]. Bruker AG-400 (Switzerland) and JEOLECX-500 (Japan) were used to measure the ^{1}H

and ^{13}C nuclear magnetic resonance spectra of the DAA derivatives using $CDCl_3$ (Anhui Zesheng Technology Co., Ltd, Energy-Chemical, China) or DMSO-d_6 (Anhui Zesheng Technology Co., Ltd, Energy-Chemical, China) as the solvent and internal standard, respectively. Related chemical shifts and coupling constants (J) were represented as parts per million and hertz, respectively. A Thermo Scientific Q Exactive UItiMate 3000 instrument was used to determine the High-resolution mass spectrometry (HRMS) of DAA derivatives. FEI Talos, F200C electron microscope (FEI, USA) images were collected using a transmission electron microscope (TEM) at a voltage of 200 kV. The morphology of phytobacteria was investigated using an FEI Nova NanoSEM 450 (FEI, USA) instrument. DAA (purity > 75%) was used as the starting material purchased from Anhui Zesheng Technology Co., Ltd, Energy-Chemical, China.

3.2. Antibacterial Activity Evaluation In Vitro and In Vivo

Analyses of the biological activity of the target molecules against the three plant bacteria *Xoo*, *Xac*, and *Psa* were performed in vitro and in vivo [62,63].

3.3. Xoo-Biofilm Formation and EPS Production Analysis

A *Xoo*-biofilm formation assay using the crystal violet staining method was performed to assess the antibacterial biofilm function of compound **2b** [14,62,63]. Initially, a 96-well plate with 200 μL of nutrient broth medium was used, and the bacterial cell suspension was adjusted to 0.1 (OD_{595nm}). Different doses of compound **2b** were added, and the mixture was incubated at 28 °C for 72 h. Following that, 200 μL of medium from each well was aspirated and washed three times with sterile water. Subsequently, bacteria were fixed with 200 μL of Carnoy's fluid for 30 min and stained with 1% crystal violet staining solution for 15 min. The crystal violet solution was then removed from the 96-well plate, and the residue was dissolved using 95% ethanol. Finally, based on the phenol-sulfuric acid standard curve, the $OD_{470\,nm}$ value was measured to determine the inhibitory effect of biofilm formation and EPS production.

3.4. Swimming Motility Assay

An examination of bacterial swimming motility was performed to assess the inhibitory effect of compound **2b** on *Xoo* cell motility. Based on previous studies but with a slight modification, *Xoo* cells suspension was adjusted to 0.2 (OD_{595nm}), and 2 μL of cell suspension was inoculated in the center of motility plates (0.3% beef extract, 0.5% peptone, 0.1% yeast powder, 1% glucose, 0.5% agar powder, and pH 7.2) with various doses (0, 1.35, 2.70, 5.40, and 10.8 μg mL^{-1}) of compound **2b** at 28 °C for 72 h. Finally, the swimming diameters for three biological replicates were observed and measured [62].

3.5. Morphology Observation of TEM

Target compound **2b** was co-incubated with bacterial cells ($OD_{595\,nm}$ = 0.1) in a shaker-incubator at 28 °C, 180 rpm for 18 h at various doses (0, 0.27, and 1.35 μg mL^{-1}) [10,52,53]. *Xoo* cells were then fixed in the copper grids and stained for TEM observation with 1% phosphotungstic acid.

3.6. Morphology Observation of Scanning Electron Microscope (SEM)

Xoo cells with an initial $OD_{595\,nm}$ = 0.1 were co-incubated with compound **2b** for 12 h at different doses (0, 25, and 50 μg mL^{-1}) in a shaker incubator (28 °C, 180 rpm). Subsequently, 2.5% glutaraldehyde was used to fix the *Xoo* cells overnight after they had been collected via centrifugation and resuspension. The glutaraldehyde solution was then removed, and the residue was dehydrated using ethanol at various concentrations (30%, 50%, 70%, 90%, and 100%). Finally, samples were freeze-dried and gold-coated for SEM observation [62,64].

3.7. Pathogenicity Assay

A pathogenicity assay assessed the bacterial virulence after 24 h of interaction between *Xoo* cells and compound **2b** at various doses (0, 0.27, 1.35, and 2.70 μg mL^{-1}). Subsequently, the *Xoo* cell suspension was adjusted to 0.5 ($OD_{595\,nm}$), and three biological replicates of rice leaves were inoculated using the leaf-clipping method [14,62]. The leaf lesion lengths were observed and measured after fourteen days, and the one-way analysis of variance was used to evaluate the lesion length data.

4. Conclusions

The rice BLB caused by *Xoo* secreting many bacterial VFs is a sustained global danger to agricultural products. Our completed research indicates that compound **2b** would be a desirable and potent bactericide candidate for preventing rice BLB by specifically targeting *Xoo*-VFs. Initially, DAA was believed to be a forestry resource with significant added value due to its wide range of biological activities. Subsequently, many novel DAA derivatives were ingeniously partially synthesized, and their anti-*Xoo* properties were evaluated in vitro. All biological analyses showed that novel DAA derivatives containing amino alcohol fragments had remarkable anti-virulence properties that functioned by inhibiting a variety of bacterial VFs, including EPS, biofilm, swimming motility, and flagella. In vivo, compound **2b** showed excellent curative and protective properties, with minimal phytotoxicity at 200 and 500 μg mL^{-1}. Finally, we made some preliminary speculations about the mechanism by which **2b** inhibited flagella and swimming motility, interfered with EPS secretion and cell adhesion, prevented biofilm formation and bacterial colonization, and decreased bacterial pathogenicity.

Supplementary Materials: The following supporting information can be downloaded at: https://www.mdpi.com/article/10.3390/ijms24032897/s1.

Author Contributions: Conceptualization, P.Q. and S.Y.; methodology, P.Q. and T.Z.; software, N.W. and Y.F.; formal analysis, D.Z.; data curation, J.M.; writing—original draft preparation, P.Q. and S.Y.; writing—review and editing, X.Z. and S.Y.; visualization, P.Q. and L.L.; supervision, X.Z., L.J. and S.Y.; project administration, X.Z. and S.Y.; funding acquisition, X.Z. and S.Y. All authors have read and agreed to the published version of the manuscript.

Funding: We acknowledge the support from the National Natural Science Foundation of China (21877021, 32160661, 32202359), the Guizhou Provincial S&T Project (2018[4007]), the Guizhou Province [Qianjiaohe KY number (2020)004], Program of Introducing Talents of Discipline to Universities of China (D20023, 111 Program) and GZU (Guizhou University) Found for Newly Enrolled Talent (No. 202229).

Institutional Review Board Statement: Not applicable.

Informed Consent Statement: Not applicable.

Data Availability Statement: Not applicable.

Conflicts of Interest: The authors declare no conflict of interest.

Abbreviations

Dehydroabietic acid	DAA
Xanthomonas oryzae pv. *oryzae*	*Xoo*
Xanthomonas. axonopodis pv *citri*	*Xac*
Pseudomonas syringae pv. *actinidiae*	*Psa*
Bacterial leaf blight	BLB
Extracellular polysaccharide	EPS
Virulence factors	VFs
Effective concentration for 50% of maximal effect	EC_{50}
Thiodiazole copper	TC

References

1. Doucoure, H.; Perez-Quintero, A.L.; Reshetnyak, G.; Tekete, C.; Auguy, F.; Thomas, E.; Koebnik, R.; Szurek, B.; Koita, O.; Verdier, V.; et al. Functional and Genome Sequence-Driven Characterization of *tal* Effector Gene Repertoires Reveals Novel Variants With Altered Specificities in Closely Related Malian *Xanthomonas oryzae* pv. *oryzae* Strains. *Front. Microbiol.* **2018**, *9*, 1657. [CrossRef] [PubMed]
2. Hou, Y.X.; Wang, L.; Wang, L.Y.; Liu, L.M.; Li, L.M.; Sun, L.; Rao, Q.; Zhang, J.; Huang, S.W. JMJ704 positively regulates rice defense response against *Xanthomonas oryzae* pv. *oryzae* infection via reducing H3K4me2/3 associated with negative disease resistance regulators. *BMC Plant Biol.* **2015**, *15*, 286. [CrossRef]
3. Xu, J.; Zhou, L.; Venturi, V.; He, Y.W.; Kojima, M.; Sakakibari, H.; Hofte, M.; De Vleesschauwer, D. Phytohormone-mediated interkingdom signaling shapes the outcome of rice-*Xanthomonas oryzae* pv. *oryzae* interactions. *BMC Plant. Biol.* **2015**, *15*, 10. [CrossRef]
4. Marimon, O.; Teixeira, J.M.; Cordeiro, T.N.; Soo, V.W.; Wood, T.L.; Mayzel, M.; Amata, I.; Garcia, J.; Morera, A.; Gay, M.; et al. An oxygen-sensitive toxin-antitoxin system. *Nat. Commun.* **2016**, *7*, 13634. [CrossRef]
5. Baker, P.; Hill, P.J.; Snarr, B.D.; Alnabelseya, N.; Pestrak, M.J.; Lee, M.J.; Jennings, L.K.; Tam, J.; Melnyk, R.A.; Parsek, M.R.; et al. Exopolysaccharide biosynthetic glycoside hydrolases can be utilized to disrupt and prevent Pseudomonas aeruginosa biofilms. *Sci. Adv.* **2016**, *2*, e1501632. [CrossRef]
6. Durgadevi, R.; Abirami, G.; Alexpandi, R.; Nandhini, K.; Kumar, P.; Prakash, S.; Veera Ravi, A. Explication of the potential of 2-hydroxy-4-methoxybenzaldehyde in hampering uropathogenic proteus mirabilis crystalline biofilm and virulence. *Front. Microbiol.* **2019**, *10*, 2804. [CrossRef] [PubMed]
7. Xuan, T.F.; Liu, J.; Wang, Z.Q.; Chen, W.M.; Lin, J. Fluorescent Detection of the Ubiquitous Bacterial Messenger 3′,5′ Cyclic Diguanylic Acid by Using a Small Aromatic Molecule. *Front. Microbiol.* **2019**, *10*, 3163. [CrossRef] [PubMed]
8. Camara-Almiron, J.; Navarro, Y.; Diaz-Martinez, L.; Magno-Perez-Bryan, M.C.; Molina-Santiago, C.; Pearson, J.R.; de Vicente, A.; Perez-Garcia, A.; Romero, D. Dual functionality of the amyloid protein TasA in Bacillus physiology and fitness on the phylloplane. *Nat. Commun.* **2020**, *11*, 1859. [CrossRef]
9. Moradali, M.F.; Ghods, S.; Rehm, B.H.A. Pseudomonas aeruginosa Lifestyle: A Paradigm for Adaptation, Survival, and Persistence. *Front. Cell. Infect. Microbiol.* **2017**, *7*, 39. [CrossRef]
10. Uchida, K.; Dono, K.; Aizawa, S. Length control of the flagellar hook in a temperature-sensitive *flgE* mutant of *Salmonella enterica* serovar Typhimurium. *J. Bacteriol.* **2013**, *195*, 3590–3595. [CrossRef]
11. Jackson, K.M.; Schwartz, C.; Wachter, J.; Rosa, P.A.; Stewart, P.E. A widely conserved bacterial cytoskeletal component influences unique helical shape and motility of the spirochete *Leptospira biflexa*. *Mol. Microbiol.* **2018**, *108*, 77–89. [CrossRef] [PubMed]
12. Weller-Stuart, T.; Toth, I.; De Maayer, P.; Coutinho, T. Swimming and twitching motility are essential for attachment and virulence of *Pantoea ananatis* in onion seedlings. *Mol. Plant Pathol.* **2017**, *18*, 734–745. [CrossRef] [PubMed]
13. Hoeflinger, J.L.; Miller, M.J. *Cronobacter sakazakii* ATCC 29544 Autoaggregation Requires FliC Flagellation, Not Motility. *Front. Microbiol.* **2017**, *8*, 301. [CrossRef] [PubMed]
14. Feng, Y.M.; Qi, P.Y.; Xiao, W.L.; Zhang, T.H.; Zhou, X.; Liu, L.W.; Yang, S. Fabrication of Isopropanolamine-Decorated Coumarin Derivatives as Novel Quorum Sensing Inhibitors to Suppress Plant Bacterial Disease. *J. Agric. Food Chem.* **2022**, *70*, 6037–6049. [CrossRef] [PubMed]
15. Liu, H.W.; Ji, Q.T.; Ren, G.G.; Wang, F.; Su, F.; Wang, P.Y.; Zhou, X.; Wu, Z.B.; Li, Z.; Yang, S. ntibacterial Functions and Proposed Modes of Action of Novel 1,2,3,4-Tetrahydro-beta-carboline Derivatives that Possess an Attractive 1,3-Diaminopropan-2-ol Pattern against Rice Bacterial Blight, Kiwifruit Bacterial Canker, and Citrus Bacterial Canker. *J. Agric. Food Chem.* **2020**, *68*, 12558–12568. [CrossRef] [PubMed]
16. Vankova, E.; Paldrychova, M.; Kasparova, P.; Lokocova, K.; Kodes, Z.; Matatkova, O.; Kolouchova, I.; Masak, J. Natural antioxidant pterostilbene as an effective antibiofilm agent, particularly for gram-positive cocci. *World J. Microbiol. Biotechnol.* **2020**, *36*, 101. [CrossRef]
17. Berger, M.; Roller, A.; Maulide, N. Synthesis and antimicrobial evaluation of novel analogues of dehydroabietic acid prepared by C-H-Activation. *Eur. J. Med. Chem.* **2017**, *126*, 937–943. [CrossRef]
18. Goodson, B.; Ehrhardt, A.; Ng, S.; Nuss, J.; Johnson, K.; Giedlin, M.; Yamamoto, R.; Moos, W.H.; Krebber, A.; Ladner, M.; et al. Characterization of Novel Antimicrobial Peptoids. Antimicrob. *Agents Chemother.* **1999**, *43*, 1429–1434. [CrossRef]
19. Fallarero, A.; Skogman, M.; Kujala, J.; Rajaratnam, M.; Moreira, V.M.; Yli-Kauhaluoma, J.; Vuorela, P. (+)-Dehydroabietic acid, an abietane-type diterpene, inhibits *Staphylococcus aureus* biofilms in vitro. *Int. J. Mol. Sci.* **2013**, *14*, 12054–12072. [CrossRef]
20. Gu, W.; Wang, S.F. Synthesis and antimicrobial activities of novel 1*H*-dibenzo[a,c]carbazoles from dehydroabietic acid. *Eur. J. Med. Chem.* **2010**, *45*, 4692–4696. [CrossRef]
21. Zhang, W.M.; Yao, Y.; Yang, T.; Wang, X.Y.; Zhu, Z.Y.; Xu, W.T.; Lin, H.X.; Gao, Z.B.; Zhou, H.; Yang, C.G.; et al. The synthesis and antistaphylococcal activity of *N*-sulfonaminoethyloxime derivatives of dehydroabietic acid. *Bioorg. Med. Chem. Lett.* **2018**, *28*, 1943–1948. [CrossRef]
22. Huang, X.; Liu, H.W.; Long, Z.Q.; Li, Z.X.; Zhu, J.J.; Wang, P.Y.; Qi, P.Y.; Liu, L.W.; Yang, S. Rational Optimization of 1,2,3-Triazole-Tailored Carbazoles As Prospective Antibacterial Alternatives with Significant In Vivo Control Efficiency and Unique Mode of Action. *J. Agric. Food Chem.* **2021**, *69*, 4615–4627. [CrossRef]

23. Xiang, M.; Song, Y.L.; Ji, J.; Zhou, X.; Liu, L.W.; Wang, P.Y.; Wu, Z.B.; Li, Z.; Yang, S. Synthesis of novel 18β-glycyrrhetinic piperazine amides displaying significant in vitro and in vivo antibacterial activities against intractable plant bacterial diseases. *Pest Manag. Sci.* **2020**, *76*, 2959–2971. [CrossRef] [PubMed]
24. Zhao, Y.L.; Huang, X.; Liu, L.W.; Wang, P.Y.; Long, Q.S.; Tao, Q.Q.; Li, Z.; Yang, S. Identification of Racemic and Chiral Carbazole Derivatives Containing an Isopropanolamine Linker as Prospective Surrogates against Plant Pathogenic Bacteria: In Vitro and In Vivo Assays and Quantitative Proteomics. *J. Agric. Food Chem.* **2019**, *67*, 7512–7525. [CrossRef]
25. Brown, L.R.; Caulkins, R.C.; Schartel, T.E.; Rosch, J.W.; Honsa, E.S.; Schultz-Cherry, S.; Meliopoulos, V.A.; Cherry, S.; Thornton, J.A. Increased Zinc Availability Enhances Initial Aggregation and Biofilm Formation of *Streptococcus pneumoniae*. *Front. Cell Infect. Microbiol.* **2017**, *7*, 233. [CrossRef]
26. Chen, W.; Liu, Y.; Zhang, L.; Gu, X.; Liu, G.; Shahid, M.; Gao, J.; Ali, T.; Han, B. *Nocardia cyriacigeogica* from Bovine Mastitis Induced In vitro Apoptosis of Bovine Mammary Epithelial Cells via Activation of Mitochondrial-Caspase Pathway. *Front. Cell Infect. Microbiol.* **2017**, *7*, 194. [CrossRef] [PubMed]
27. Seijsing, F.; Nileback, L.; Ohman, O.; Pasupuleti, R.; Stahl, C.; Seijsing, J.; Hedhammar, M. Recombinant spider silk coatings functionalized with enzymes targeting bacteria and biofilms. *Microbiologyopen* **2020**, *9*, e993. [CrossRef]
28. Liu, Z.D.; Schade, R.; Luthringer, B.; Hort, N.; Rothe, H.; Muller, S.; Liefeith, K.; Willumeit-Romer, R.; Feyerabend, F. Influence of the Microstructure and Silver Content on Degradation, Cytocompatibility, and Antibacterial Properties of Magnesium-Silver Alloys In Vitro. *Oxid. Med. Cell Longev.* **2017**, *2017*, 8091265. [CrossRef]
29. Zeng, X.H.; She, P.F.; Zhou, L.Y.; Li, S.J.; Hussain, Z.; Chen, L.H.; Wu, Y. Drug repurposing: Antimicrobial and antibiofilm effects of penfluridol against *Enterococcus faecalis*. *Microbiologyopen* **2021**, *10*, e1148. [CrossRef]
30. Zheng, J.X.; Lin, Z.W.; Chen, C.; Chen, Z.; Lin, F.J.; Wu, Y.; Yang, S.Y.; Sun, X.; Yao, W.M.; Li, D.Y.; et al. Biofilm Formation in *Klebsiella pneumoniae* Bacteremia Strains Was Found to be Associated with CC23 and the Presence of *wcaG*. *Front. Cell Infect. Microbiol.* **2018**, *8*, 21. [CrossRef] [PubMed]
31. Zhang, Y.Y.; Chen, X.; Gueydan, C.; Han, J.H. Plasma membrane changes during programmed cell deaths. *Cell Res.* **2018**, *28*, 9–21. [CrossRef]
32. Wanyi Tai, P.Z.; Gao, X.H. Cytosolic delivery of proteins by cholesterol tagging. *Sci. Adv.* **2020**, *6*, eabb0310.
33. Costa, O.Y.A.; de Hollander, M.; Pijl, A.; Liu, B.; Kuramae, E.E. Cultivation-independent and cultivation-dependent metagenomes reveal genetic and enzymatic potential of microbial community involved in the degradation of a complex microbial polymer. *Microbiome* **2020**, *8*, 76. [CrossRef]
34. Rajput, A.; Thakur, A.; Sharma, S.; Kumar, M. aBiofilm: A resource of anti-biofilm agents and their potential implications in targeting antibiotic drug resistance. *Nucleic Acids Res.* **2018**, *46*, D894–D900. [CrossRef]
35. Yao, J.; Allen, C. Chemotaxis is required for virulence and competitive fitness of the bacterial wilt pathogen *Ralstonia solanacearum*. *J. Bacteriol.* **2006**, *188*, 3697–3708. [CrossRef]
36. Kurre, R.; Maier, B. Oxygen Depletion Triggers Switching between Discrete Speed Modes of Gonococcal Type IV Pili. *Biophys. J.* **2012**, *102*, 2556–2563. [CrossRef] [PubMed]
37. Mideros-Mora, C.; Miguel-Romero, L.; Felipe-Ruiz, A.; Casino, P.; Marina, A. Revisiting the pH-gated conformational switch on the activities of HisKA-family histidine kinases. *Nat. Commun.* **2020**, *11*, 769. [CrossRef] [PubMed]
38. Zhu, S.W.; Nishikino, T.; Takekawa, N.; Terashima, H.; Kojima, S.; Imada, K.; Homma, M.; Liu, J. In Situ Structure of the *Vibrio* Polar Flagellum Reveals a Distinct Outer Membrane Complex and Its Specific Interaction with the Stator. *J. Bacteriol.* **2020**, *202*, 4. [CrossRef] [PubMed]
39. Li, B.Y.; Huang, Q.; Cui, A.L.; Liu, X.L.; Hou, B.; Zhang, L.Y.; Liu, M.; Meng, X.R.; Li, S.W. Overexpression of Outer Membrane Protein X (OmpX) Compensates for the Effect of TolC Inactivation on Biofilm Formation and Curli Production in Extraintestinal Pathogenic *Escherichia coli* (ExPEC). *Front. Cell Infect. Microbiol.* **2018**, *8*, 208. [CrossRef]
40. Sun, W.X.; Dunning, F.M.; Pfund, C.; Weingarten, R.; Bent, A.F. Within-species flagellin polymorphism in *Xanthomonas campestris* pv *campestris* and its impact on elicitation of Arabidopsis *FLAGELLIN SENSING2*-dependent defenses. *Plant Cell* **2006**, *18*, 764–779. [CrossRef] [PubMed]
41. Kan, J.H.; An, L.; Wu, Y.; Long, J.; Song, L.Y.; Fang, R.X.; Jia, Y.T. A dual role for proline iminopeptidase in the regulation of bacterial motility and host immunity. *Mol. Plant Pathol.* **2018**, *19*, 2011–2024. [CrossRef] [PubMed]
42. McKee, R.W.; Mangalea, M.R.; Purcell, E.B.; Borchardt, E.K.; Tamayo, R. The second messenger cyclic Di-GMP regulates *Clostridium difficile* toxin production by controlling expression of *sigD*. *J. Bacteriol.* **2013**, *195*, 5174–5185. [CrossRef] [PubMed]
43. Vannuccini, E.; Paccagnini, E.; Cantele, F.; Gentile, M.; Dini, D.; Fino, F.; Diener, D.; Mencarelli, C.; Lupetti, P. Two classes of short intraflagellar transport train with different 3D structures are present in *Chlamydomonas* flagella. *J. Cell Sci.* **2016**, *129*, 2064–2074.
44. Agarwal, A.; Guthrie, K.M.; Czuprynski, C.J.; Schurr, M.J.; McAnulty, J.F.; Murphy, C.J.; Abbott, N.L. Polymeric Multilayers that contain Silver Nanoparticles can be Stamped onto Biological Tissues to Provide Antibacterial Activity. *Adv. Funct. Mater.* **2011**, *21*, 1863–1873. [CrossRef]
45. An, J.P.; Wang, X.F.; Zhang, X.W.; Xu, H.F.; Bi, S.Q.; You, C.X.; Hao, Y.J. An apple MYB transcription factor regulates cold tolerance and anthocyanin accumulation and undergoes MIEL1-mediated degradation. *Plant Biotechnol. J.* **2020**, *18*, 337–353. [CrossRef] [PubMed]
46. Sims, K.R.; Liu, Y.; Hwang, G.; Jung, H.I.; Koo, H.; Benoit, D.S.W. Enhanced design and formulation of nanoparticles for anti-biofilm drug delivery. *Nanoscale* **2018**, *11*, 219–236. [CrossRef]

47. Wu, G.H.; Majewski, J.; Ege, C.; Kjaer, K.; Weygand, M.J.; Lee, K.Y. Interaction between lipid monolayers and poloxamer 188: An X-ray reflectivity and diffraction study. *Biophys. J.* **2005**, *89*, 3159–3173. [CrossRef]
48. Raguz, M.; Mainali, L.; O'Brien, W.J.; Subczynski, W.K. Lipid domains in intact fiber-cell plasma membranes isolated from cortical and nuclear regions of human eye lenses of donors from different age groups. *Exp. Eye Res.* **2015**, *132*, 78–90. [CrossRef]
49. Pang, R.; Xie, T.F.; Wu, Q.P.; Li, Y.P.; Lei, T.; Zhang, J.M.; Ding, Y.; Wang, J.; Xue, L.; Chen, M.T.; et al. Comparative Genomic Analysis Reveals the Potential Risk of *Vibrio parahaemolyticus* Isolated From Ready-To-Eat Foods in China. *Front. Microbiol.* **2019**, *10*, 186. [CrossRef]
50. Imperi, F.; Leoni, L.; Visca, P. Antivirulence activity of azithromycin in *Pseudomonas aeruginosa*. *Front. Microbiol.* **2014**, *5*, 178. [CrossRef]
51. Ueda, M.; Egoshi, S.; Dodo, K.; Ishimaru, Y.; Yamakoshi, H.; Nakano, T.; Takaoka, Y.; Tsukiji, S.; Sodeoka, M. Noncanonical Function of a Small-Molecular Virulence Factor Coronatine against Plant Immunity: An In Vivo Raman Imaging Approach. *ACS Cent. Sci.* **2017**, *3*, 462–472. [CrossRef]
52. Taguchi, F.; Suzuki, T.; Inagaki, Y.; Toyoda, K.; Shiraishi, T.; Ichinose, Y. The siderophore pyoverdine of *Pseudomonas syringae* pv. *tabaci* 6605 is an intrinsic virulence factor in host tobacco infection. *J. Bacteriol.* **2010**, *192*, 117–126. [CrossRef] [PubMed]
53. Mahamat Abdelrahim, A.; Radomski, N.; Delannoy, S.; Djellal, S.; Le Negrate, M.; Hadjab, K.; Fach, P.; Hennekinne, J.A.; Mistou, M.Y.; Firmesse, O. Large-Scale Genomic Analyses and Toxinotyping of *Clostridium perfringens* Implicated in Foodborne Outbreaks in France. *Front. Microbiol.* **2019**, *10*, 777. [CrossRef] [PubMed]
54. Li, R.F.; Wang, X.X.; Wu, L.; Huang, L.; Qin, Q.J.; Yao, J.L.; Lu, G.T.; Tang, J.L. *Xanthomonas campestris* sensor kinase HpaS co-opts the orphan response regulator VemR to form a branched two-component system that regulates motility. *Mol. Plant Pathol.* **2020**, *21*, 360–375. [CrossRef] [PubMed]
55. Shen, F.F.; Yin, W.F.; Song, S.H.; Zhang, Z.H.; Ye, P.Y.; Zhang, Y.; Zhou, J.N.; He, F.; Li, P.; Deng, Y.Y. *Ralstonia solanacearum* promotes pathogenicity by utilizing L-glutamic acid from host plants. *Mol. Plant Pathol.* **2020**, *21*, 1099–1110. [CrossRef]
56. Hamdoun, S.; Gao, M.; Gill, M.; Kwon, A.; Norelli, J.L.; Lu, H. Signalling requirements for *Erwinia amylovora*-induced disease resistance, callose deposition and cell growth in the non-host *Arabidopsis thaliana*. *Mol. Plant Pathol.* **2018**, *19*, 1090–1103. [CrossRef]
57. Wei, Y.; Caceres-Moreno, C.; Jimenez-Gongora, T.; Wang, K.K.; Sang, Y.Y.; Lozano-Duran, R.; Macho, A.P. The *Ralstonia solanacearum* csp22 peptide, but not flagellin-derived peptides, is perceived by plants from the *Solanaceae* family. *Plant Biotechnol. J.* **2018**, *16*, 1349–1362. [CrossRef]
58. Dong, O.X.; Ronald, P.C. Genetic Engineering for Disease Resistance in Plants: Recent Progress and Future Perspectives. *Plant Physiol.* **2019**, *180*, 26–38. [CrossRef]
59. Fleitas Martinez, O.; Cardoso, M.H.; Ribeiro, S.M.; Franco, O.L. Recent advances in anti-virulence therapeutic strategies with a focus on dismantling bacterial membrane microdomains, toxin neutralization, quorum-sensing interference and biofilm inhibition. *Front. Cell Infect. Microbiol.* **2019**, *9*, 74. [CrossRef]
60. Ferro, T.A.; Araujo, J.M.; Dos Santos Pinto, B.L.; Dos Santos, J.S.; Souza, E.B.; da Silva, B.L.; Colares, V.L.; Novais, T.M.; Filho, C.M.; Struve, C.; et al. *Cinnamaldehyde* Inhibits *Staphylococcus aureus* Virulence Factors and Protects against Infection in a *Galleria mellonella* Model. *Front. Microbiol.* **2016**, *7*, 2052. [CrossRef]
61. Wang, G.G.; Gao, Y.W.; Wu, X.H.; Gao, X.E.; Zhang, M.; Liu, H.M.; Fang, T.Q. Inhibitory Effect of Piceatannol on *Streptococcus suis* Infection Both in vitro and in vivo. *Front. Microbiol.* **2020**, *11*, 593588. [CrossRef] [PubMed]
62. Qi, P.Y.; Zhang, T.H.; Feng, Y.M.; Wang, M.W.; Shao, W.B.; Zeng, D.; Jin, L.H.; Wang, P.Y.; Zhou, X.; Yang, S. Exploring an Innovative Strategy for Suppressing Bacterial Plant Disease: Excavated Novel Isopropanolamine-Tailored Pterostilbene Derivatives as Potential Antibiofilm Agents. *J. Agric. Food Chem.* **2022**, *70*, 4899–4911. [CrossRef] [PubMed]
63. Song, Y.L.; Liu, S.S.; Yang, J.; Xie, J.; Zhou, X.; Wu, Z.B.; Liu, L.W.; Wang, P.Y.; Yang, S. Discovery of Epipodophyllotoxin-Derived B_2 as Promising XooFtsZ Inhibitor for Controlling Bacterial Cell Division: Structure-Based Virtual Screening, Synthesis, and SAR Study. *Int. J. Mol. Sci.* **2022**, *23*, 9119. [CrossRef] [PubMed]
64. Wang, F.; Yang, B.X.; Zhang, T.H.; Tao, Q.Q.; Zhou, X.; Wang, P.Y.; Yang, S. Novel 1,3,4-oxadiazole thioether and sulfone derivatives bearing a flexible N-heterocyclic moiety: Synthesis, characterization, and anti-microorganism activity. *Arabian J. Chem.* **2023**, *16*, 2. [CrossRef]